JOURNAL OF MATERIALS SCIENCE 27 (1992) 233–239

Coating of titanium carbide films on stainless steel by chemical vapour deposition and their corrosion behaviour in a Br_2–O_2–Ar atmosphere

TAKASHI GOTO, CHEN-YAN GUO, HAJIME TAKEYA, TOSHIO HIRAI
Institute for Materials Research, Tohoku University, 2-1-1 Katahira Sendai 980, Japan

Stainless steel (SUS304) plates were coated with TiC films using chemical vapour deposition (CVD) as a candidate material for "UT-3" which is a promising process of hydrogen production through the thermal decomposition of water. The corrosion behaviour of the TiC film-coated SUS304 plates was examined in a Br_2–O_2–Ar atmosphere. The effects of CVD conditions on the surface texture, deposition rates and preferred orientation of the TiC films were investigated, and the optimum CVD conditions determined. Corrosion of the TiC film-coated SUS304 plates in the Br_2–O_2–Ar atmosphere was mainly caused by oxidation of the TiC film and SUS304 substrate. Microcracks in the TiC films lead to corrosion of the SUS304 substrate. At oxygen partial pressures below 0.1 kPa, weight loss was observed due to the formation of volatile titanium and iron bromides. At oxygen partial pressures greater 0.1 kPa, the time dependence of weight increase was parabolic due to the formation of oxide scale. The oxide scales were mixtures of TiO_2, Fe_2O_3 and Fe_3O_4. The corrosion mechanism is discussed thermodynamically.

1. Introduction

Hydrogen is expected to be a new energy resource because fossil fuels, i.e. oil, coal, etc., will become scarce in the near future. Hydrogen may also resolve the problem of acid rain destroying the environment. Several methods of producing hydrogen have been proposed, and the thermal decomposition of water, "UT-3", is one of the most promising processes [1]. In the "UT-3" process, the high-temperature corrosion of structural materials is an important problem because highly corrosive gases such as bromine, oxygen, hydrogen bromide, etc., should be used at around 1000 K [2]. For practical applications, structural materials such as vessels, pipes, etc., should be metals, because large chemical plants cannot be constructed from ceramics. However, no metal is known to withstand satisfactorily the corrosive environments in the "UT-3" process.

So far, many methods such as thermal spraying [3], dip coating [4], chemical vapour deposition (CVD) [5], etc., have been tried to improve the corrosion resistances of metals, and CVD is a suitable technique because pin-hole and crack-free films can be prepared by CVD.

In the past, titanium nitride (TiN), titanium carbide (TiC), silica (SiO_2) and zirconia (ZrO_2), etc., have been prepared as coatings for metals [6]. TiC films are most widely used as coatings for cutting tools because TiC is highly adhesive to metals [7]. A few reports in which CVD is applied to improve the corrosion resistance of metals have been published (e.g. [8]); however, the corrosion rates and the corrosion mechanism have not been examined.

In the present work, TiC films were coated by CVD on stainless steel (SUS304) substrates under various conditions, and the effects of CVD conditions on the microstructure and deposition rates were studied. The corrosion behaviour of the TiC film-coated SUS304 in a Br_2–O_2–Ar atmosphere was investigated and the corrosion mechanism is thermodynamically discussed.

2. Experimental procedure

2.1. Preparation of TiC films

Fig. 1 shows a schematic diagram of the preparation apparatus for CVD TiC films. Source gases $TiCl_4$, CH_4 and H_2 were introduced into a hot-wall type CVD furnace. Stainless steel (SUS304) discs (15 mm diameter and 1.5 mm thick) were used as substrates. Deposition temperatures, T_{dep}, were changed from 1173–1473 K, and the total gas pressure, P_{tot}, was fixed at 101 kPa. $TiCl_4$ vapour flow rates, FR($TiCl_4$), were controlled from 9.3–38.3×10^{-8} $m^3 s^{-1}$ by changing the temperature of the $TiCl_4$ reservoir from 273–283 K. CH_4 gas flow rates, FR(CH_4), were changed from 1.6×10^{-8}–6.2×10^{-6} $m^3 s^{-1}$, and the $CH_4/TiCl_4$ molar ratio ($m_{C/Ti}$) ranged from 0.17–17. Table I summarizes the CVD conditions for the preparation of TiC films.

The structure of CVD TiC films was examined by X-ray diffraction (XRD), the surface texture observed

0022–2461/92 $03.00 + .12

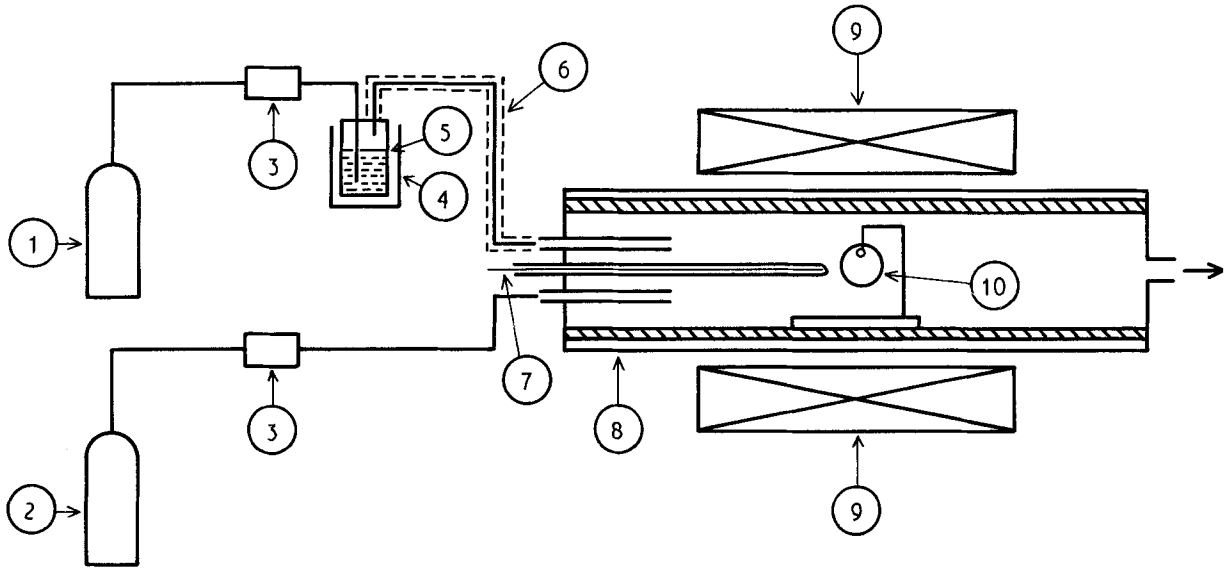

Figure 1 CVD apparatus for the preparation of TiC films. 1, H_2 gas; 2, CH_4 gas; 3, gas flow meter; 4, constant temperature bath; 5, $TiCl_4$ reservoir; 6, ribbon heater; 7, thermocouple; 8, reaction tube; 9, electric furnace; 10, substrate.

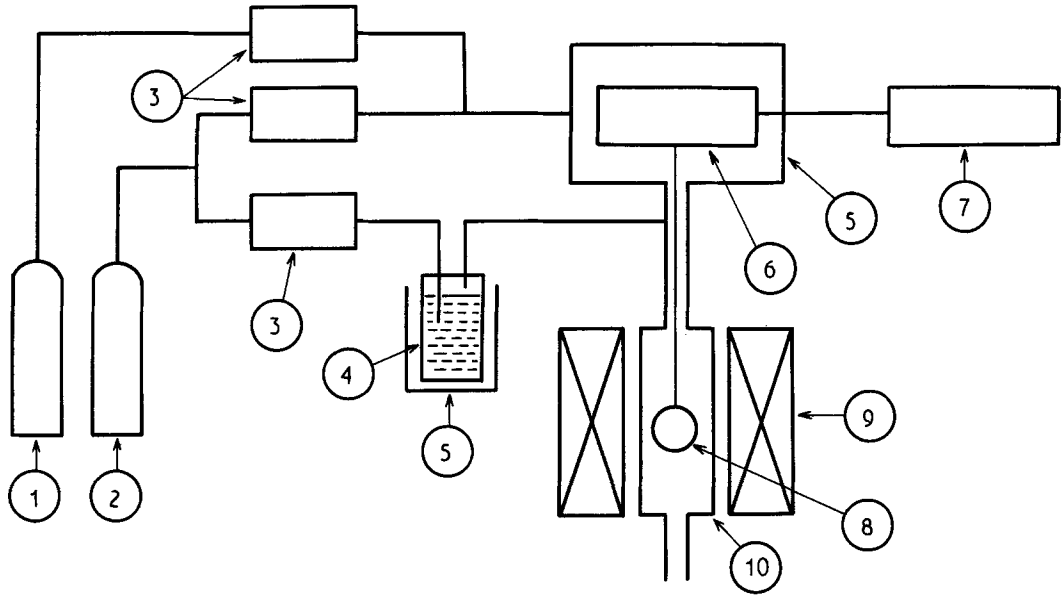

Figure 2 Schematic diagram of thermogravimetry for the measurement of corrosion rates. 1, argon gas; 2, oxygen gas; 3, gas flow meter; 4, bromine liquid; 5, constant temperature bath; 6, balance; 7, microcomputer; 8, specimen; 9, electric furnace; 10, measurement cell.

TABLE I Deposition conditions

Deposition temperature, T_{dep}	1173–1473 K
Total gas pressure, P_{tot}	101 kPa
Gas flow rate, FR	
H_2	8.3×10^{-6} m^3 s^{-1}
$TiCl_4$	9.3×10^{-8}–3.8×10^{-7} m^3 s^{-1}
CH_4	1.6×10^{-8}–6.2×10^{-6} m^3 s^{-1}
$CH_4/TiCl_4$, $m_{C/Ti}$	0.17–17
Time	21.6–28.8 ks

by optical microscopy and scanning electron microscopy (SEM), and the film thickness was determined by SEM and a Talystep thickness tester.

2.2. Measurement of corrosion rates

Fig. 2 shows a schematic diagram of thermogravimetry for the measurement of corrosion rates. The specimens were placed in an electric furnace, and a platinum wire was used to suspend the specimen. Weight changes were continuously measured using a balance which was connected to a microcomputer. The balance was kept at 288 K in a constant temperature box. Argon or oxygen gas was passed through the balance and introduced from the top of the measurement cell. Oxygen or argon gas containing bromine vapour was introduced from the bottom of the measurement cell. The bromine liquid reservoir was maintained between 273 and 288 K, and its vapour pressure (P_{Br_2}) controlled between 0 and 9 kPa. The oxygen partial pressure, P_{O_2}, ranged up to 97 kPa by controlling the mixing ratio of argon to oxygen gas. The corrosion temperatures, T_{cor}, ranged from 973–1173 K, and the total pressure was maintained at 101 kPa. The corrosion conditions are summarized in Table II.

TABLE II Corrosion conditions

Corrosion temperature, T_{cor}	973–1173 K
Br_2 partial pressure, P_{Br_2}	0–9 kPa
O_2 partial pressure, P_{O_2}	0–9.7 kPa
Total gas pressure	101 kPa
Time	0–28.8 ks

3. Results and discussion

3.1. Preparation of TiC films

Fig. 3 shows the effects of CVD conditions on the appearance of the TiC films. Below $T_{dep} = 1250$ K, soot-like not-dense deposits were obtained independent of $CH_4/TiCl_4$ ratio. Above $T_{dep} = 1250$ K, silver-coloured dense CVD TiC films were obtained. The CVD TiC films prepared at higher T_{dep} and $CH_4/TiCl_4$ ratios peeled from the SUS304 substrates. This was caused by thermal stress. The thermal expansion coefficients of TiC and SUS304 are 7.6×10^{-6} and 16.4×10^{-6}, respectively. This difference leads to large thermal stresses during the cooling step [8].

The effect of $CH_4/TiCl_4$ ratio on the preferred orientation of CVD TiC films is depicted in Fig. 4. The texture coefficients, TC, were calculated from [9]

$$TC = \frac{P - P_0}{1 - P_0} \quad (1)$$

and

$$P = \frac{I(h'k'l')}{\Sigma I(hkl)} \quad (2)$$

where $\Sigma I(hkl)$ is the summation of X-ray intensities from all (hkl) peaks, $I(h'k'l')$ is the X-ray intensity from the oriented $(h'k'l')$ plane, P_0 is the P value calculated from non-oriented specimen which is the same as that of the powder pattern. The (1 1 0) plane of CVD TiC films was almost parallel to the substrate surface at lower $CH_4/TiCl_4$ ratios, and the (1 1 1) orientation became dominant with increasing $CH_4/TiCl_4$ ratio. There have been many reports on the coating of CVD TiC films on steel substrates. Derre *et al.* [10] reported the (1 1 1) orientation, Takahashi *et al.* [11] reported the (1 1 0) and (1 1 1) orientations, and Brossa *et al.* [12] and Yoon *et al.* [13] reported the (1 0 0) and (1 1 0) orientations. However, the effects of CVD conditions on the preferred orientation are not well understood. The similar tendency mentioned above was reported by the present authors in the preparation of thick CVD TiC [14] and SiC [15] plates using $TiCl_4 + CCl_4 + H_2$ and $SiCl_4 + C_3H_8 + H_2$ gases, respectively. This behaviour may be explained by the change of supersaturation in the gas phase [16].

Fig. 5 shows the effect of the $CH_4/TiCl_4$ ratio on the surface texture of CVD TiC films prepared at $T_{dep} = 1273$ K. The (1 1 0) and (1 0 0) orientations were dominant in the films shown in Fig. 5a and b, respectively. The cubic grains shown in Fig. 5c correspond well with the character of the (1 0 0) planes of cubic cells. Many triangle facets were observed in the side of pyramidal grains. This morphology indicates that the sides of each grain could be (1 1 1) planes. Straten *et al.* [17] also reported similar surface textures for CVD TiC films prepared on steel substrates.

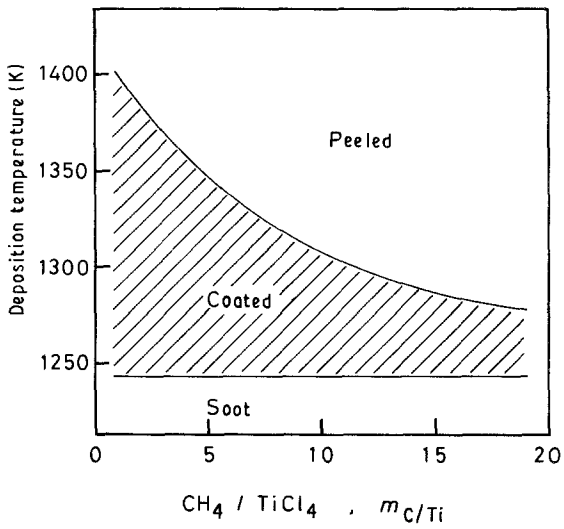

Figure 3 Effect of CVD conditions on the appearance of TiC films.

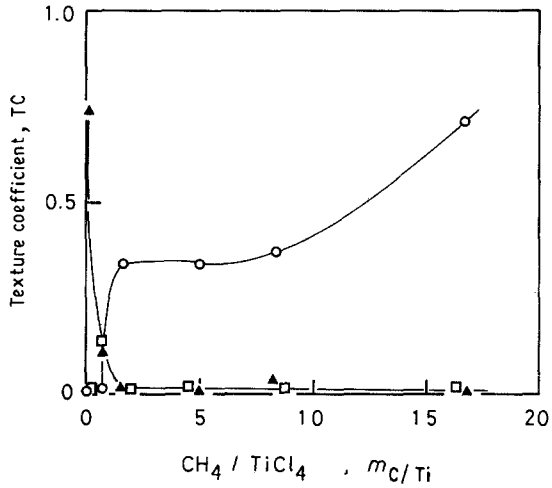

Figure 4 Effect of $CH_4/TiCl_4$ ratio on the texture coefficient. (○) TC (1 0 0), (▲) TC (1 1 0), (□) TC (1 1 1).

Fig. 6 shows the effect of the $CH_4/TiCl_4$ ratio on the deposition rates of CVD TiC films. Deposition rates increased with increasing T_{dep} and $CH_4/TiCl_4$ ratios. TiC films were obtained without introducing CH_4 gas at every T_{dep}. Takahashi *et al.* [18] also reported that the TiC films were prepared by CVD on steel substrates at $T_{dep} = 1100$–1300 K using $TiCl_4$ vapour without any carbon source gas. It was reported that the reaction between carbon in steels and $TiCl_4$ vapour should lead to TiC formation. The effect of the $TiCl_4$ vapour flow rate on the deposition rates of CVD TiC films is shown in Fig. 7. The deposition rates increased with increasing $TiCl_4$ vapour flow rate, independent of the $CH_4/TiCl_4$ ratio and T_{dep}. The largest deposition rate obtained in the present work was 4 nm s^{-1} at $T_{dep} = 1273$ K, $CH_4/TiCl_4$ ratio = 17 and $TiCl_4$ vapour flow rate = 4.2×10^{-7} m^3 s^{-1}. This value was larger than 0.4 nm s^{-1} obtained by

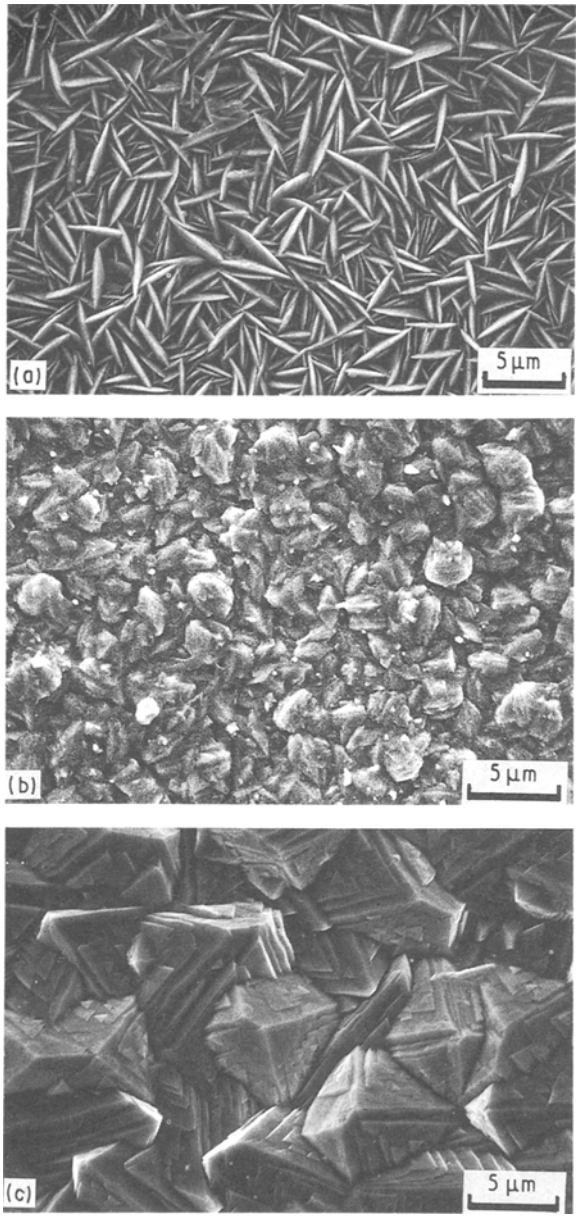

Figure 5 Effect of $CH_4/TiCl_4$ ratio on the surface texture of TiC films at $T_{dep} = 1273$ K, $FR(TiCl_4) = 1.0 \times 10^{-7}$ m^3 s^{-1} and $CH_4/TiCl_4$ = (a) 0.17, (b) 0.86, and (c) 17.

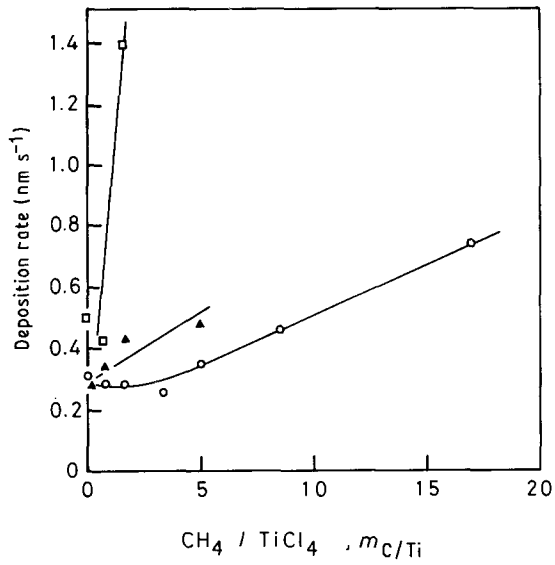

Figure 6 Effect of $CH_4/TiCl_4$ ratio on the deposition rate of TiC films. T_{dep}: (○) 1273 K, (▲) 1323 K, (□) 1373 K.

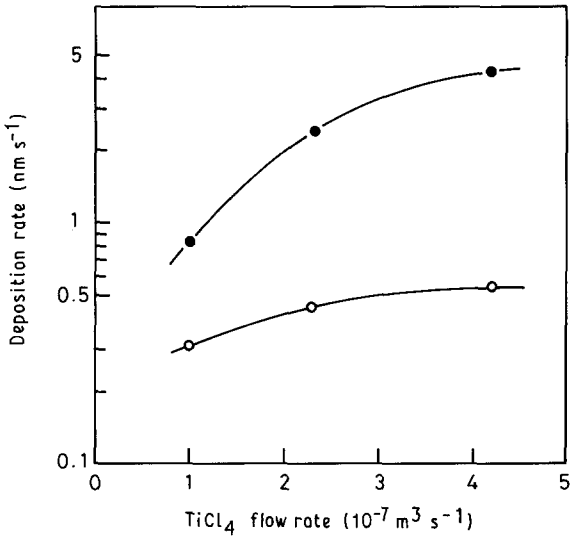

Figure 7 Effect of $TiCl_4$ flow rate on the deposition rate at $T_{dep} = 1273$ K. $m_{C/Ti}$: (○) 1.7, (●) 17.

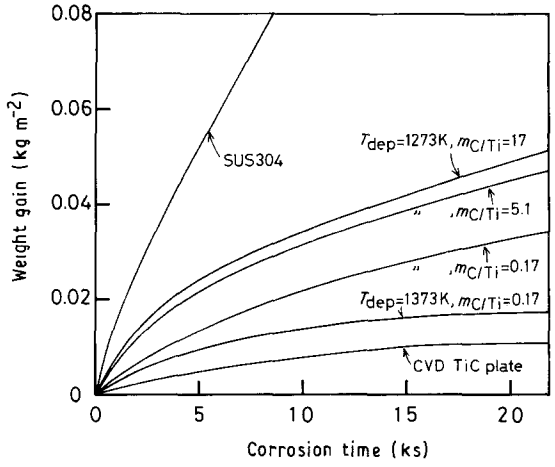

Figure 8 Relationship between time and weight gain by the corrosion at $T_{cor} = 1073$ K, $P_{Br_2} = 4.4$ kPa and $P_{O_2} = 46$ kPa.

Tsuchiya *et al.* at $T_{dep} = 1293$ K on SUS304 substrates [19], but was smaller than 13.3 nm s^{-1} obtained by Takahashi *et al.* at $T_{dep} = 1273$ K on steel substrates [11]. These values depend on the geometry of the CVD furnace and source gas flow rates, etc.

3.2. Corrosion behaviour

Fig. 8 shows the relationship between time and weight gain per unit surface area for SUS304 and TiC-coated SUS304 in a Br_2–O_2–Ar atmosphere. The weight gain for high-purity thick CVD TiC plates were shown for comparison. The weights of SUS304 increased linearly with time after approximately 2 ks, and those of TiC-coated SUS304 increased parabolically. At $T_{dep} = 1273$ K, the weight gain increased with increasing $CH_4/TiCl_4$ ratio. At $CH_4/TiCl_4 = 0.17$, the weight gain decreased with increasing T_{dep}. The weight gain of the thick CVD TiC plates was smaller than that of TiC-coated SUS304, and the surface scales formed on the TiC-coated SUS304 by the corrosion were identified as TiO_2 (rutile), Fe_2O_3 and Fe_3O_4. These results

could explain why SUS304 corroded through microcracks in the TiC films, and also why the weight gain of the TiC-coated SUS304 was larger than that of the thick CVD TiC plates. The difference in weight gain shown in Fig. 8 may depend on the number of microcracks in the CVD TiC films. The weight gain of the TiC-coated SUS304 apparently obeyed a parabolic law. This result suggests that the number of microcracks remain constant during the corrosion time. The specimen prepared at $T_{dep} = 1373$ K, $CH_4/TiCl_4 = 0.17$ and $TiCl_4$ vapour flow rate $= 4.2 \times 10^{-7}\ m^3\ s^{-1}$ (deposition time 6 h, thickness $\sim 10^{-2}$ mm) had the highest corrosion resistance, as shown in Fig. 8. Further corrosion experiments have been conducted using the specimens prepared under these CVD conditions.

Fig. 9 shows Arrhenius plots of corrosion rates (parabolic rate constants, K_p). The relationship between $\log K_p$ and $1/T$ was linear, independent of bromine partial pressure, and the apparent activation energy was 120–160 kJ mol^{-1}. Fig. 10 shows the effect of P_{O_2} on K_p. The values of K_p increased with increasing P_{O_2}, independent of T_{cor}. These results show that the rate-determining step could be the diffusion of oxygen in the oxide scale. More detailed discussion of the corrosion kinetics is difficult because the oxide scales have complicated compositions consisting of TiO_2, Fe_2O_3 and Fe_3O_4.

The effect of P_{Br_2} on K_p is shown in Fig. 11. Bromine vapour did not affect the corrosion rates below $P_{Br_2} = 5$ kPa; however, at $P_{Br_2} = 9$ kPa the value of K_p significantly increased. It is well known that bromine vapour accelerates the corrosion of stainless steels [20]. This should mean that K_p is larger at higher P_{Br_2}. At $P_{O_2} < 0.1$ kPa, weight loss was observed as shown in Fig. 12; at the same time, titanium and iron bromides were formed in the lower temperature regions of the measurement cell.

Figs 13 and 14 demonstrate the thermodynamic analyses for the corrosion of TiC-coated SUS304 in the Br_2–O_2–Ar atmosphere. In order to simplify the analysis, SUS304 was assumed to be iron; therefore, an Fe–TiC–Br_2–O_2–Ar system was investigated in the present calculations. Fig. 13 shows the effects of P_{Br_2} and P_{O_2} on equilibrium solid phases at $T_{cor} = 1100$ K.

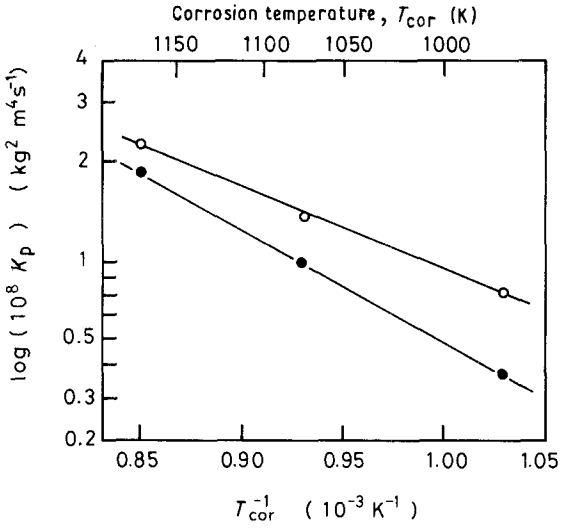

Figure 9 Arrhenius plot of the corrosion rates (parabolic rate constants) at $P_{O_2} = 0.15$ kPa. P_{Br_2}: (○) 4.4 kPa, (●) 1.8 kPa.

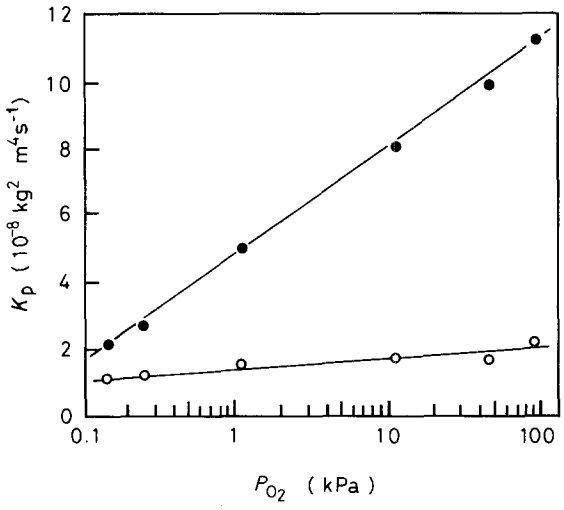

Figure 10 Effect of oxygen partial pressure on the corrosion rates (parabolic rate constants) at $P_{Br_2} = 4.4$ kPa. T_{cor}: (○) 1073 K, (●) 1173 K.

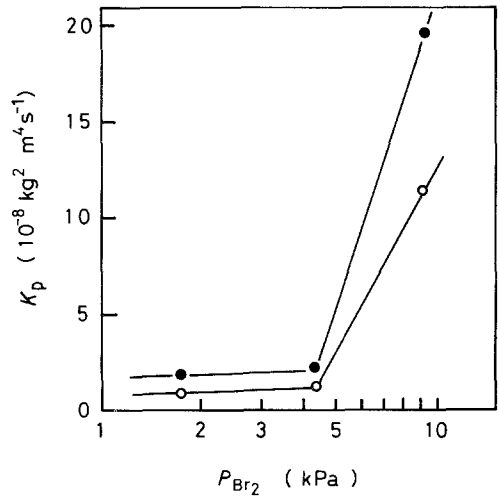

Figure 11 Effect of bromine partial pressure on the corrosion rates (parabolic rate constants) at $P_{O_2} = 0.15$ kPa. T_{cor}: (○) 1073 K, (●) 1173 K.

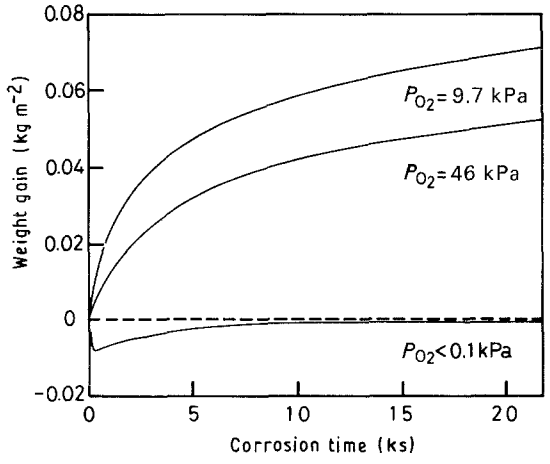

Figure 12 Relationship between time and weight gain by the corrosion at $T_{cor} = 1173$ K and $P_{Br_2} = 4.4$ kPa.

TABLE III Gas and solid species used in the thermodynamic calculations

Gas species	Solid species
Ar Ti C C_2 C_3 TiO TiO_2 Br Br_2	Ti TiO TiO_2 TiO_3 Ti_3O_5 Ti_4O_7 $TiBr_2$
TiBr $TiBr_2$ $TiBr_3$ $TiBr_4$ O O_2 O_3	$TiBr_3$ $TiBr_4$ C TiC Fe FeO Fe_2O_3
CO CO_2 C_2O C_3O_2 Fe $FeBr_2$ $FeBr_4$	Fe_3O_4 $FeBr_2$

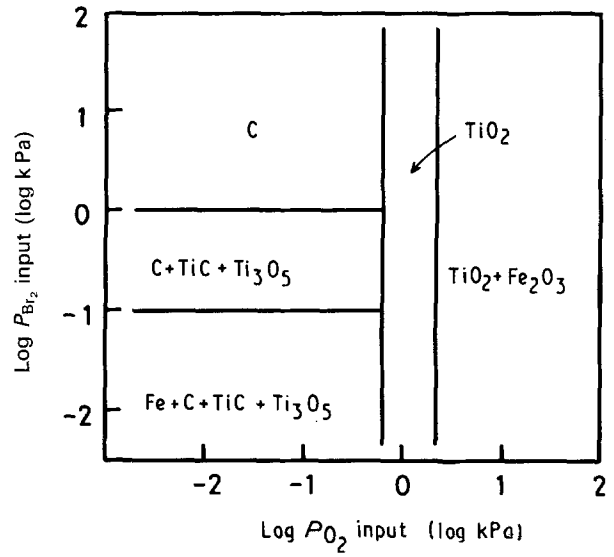

Figure 13 Effects of P_{Br_2} and P_{O_2} on the equilibrium solid phases calculated at T_{cor} = 1100 K.

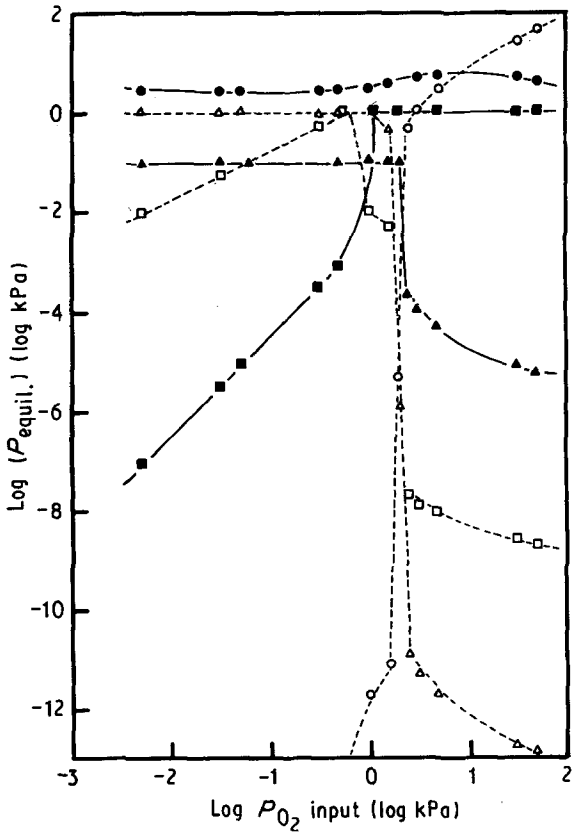

Figure 14 Effect of P_{O_2} input and equilibrium partial pressures of gas species at T_{cor} = 1100 K and P_{Br_2} = 5 kPa. (○) O_2, (●) Br_2, (△) $TiBr_4$, (▲) $FeBr_2$, (□) CO, (■) CO_2.

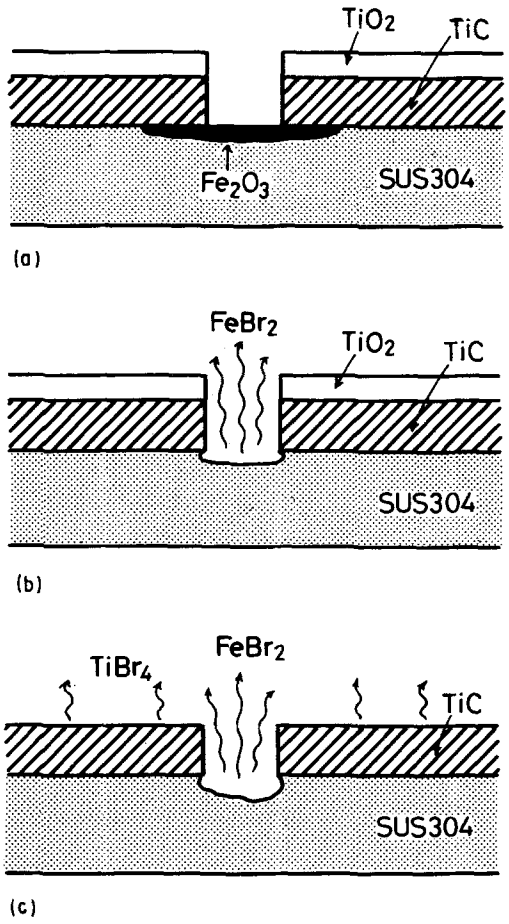

Figure 15 Schematic diagram of the effect of $P_{O_2\ input}$ on the corrosion behaviour at T_{cor} = 1100 K and P_{Br_2} = 5 kPa. (a) $P_{O_2\ input} > 2.5$ kPa, (b) 0.5 kPa $< P_{O_2\ input} < 2.5$ kPa, (c) $P_{O_2\ input} < 0.5$ kPa.

The computer code SOLGASMIX-PV [21] and the JANAF thermochemical data [22] were used for the calculations. The gas and solid species assumed are summarized in Table III.

Fig. 14 shows the relationship between input oxygen partial pressure ($P_{O_2\ input}$) and equilibrium partial pressure of gas species at P_{Br_2} = 5 kPa. At more than P_{O_2} = 2.5 kPa, both iron and TiC should be oxidized to TiO_2 and Fe_2O_3, and protective scales could be formed. At 0.5 kPa $< P_{O_2\ input} <$ 2.5 kPa, TiC should be oxidized to TiO_2 but iron should react with bromine to form volatile $FeBr_2$. At $P_{O_2\ input} <$ 0.5 kPa, the protective oxide scale could not be formed, and weight loss due to the formation of $TiBr_4$ and $FeBr_2$ should be observed. Fig. 15 shows a schematic diagram of the effect of P_{O_2} on the corrosion behaviour of TiC-coated SUS304. When P_{O_2} was less than about 0.1 kPa, rapid weight loss was initially observed and then the weight gradually increased with time as shown in Fig. 12.

This behaviour could correspond with Fig. 15b. At $P_{O_2} = 46$ and 97 kPa shown in Fig. 12, the corrosion behaviour could be explained by Fig. 15a. When P_{O_2} was higher, a larger weight gain was observed. This suggests that the oxide scales formed at higher P_{O_2} could not be more protective.

4. Conclusions

TiC films were coated on stainless steel (SUS304) by CVD using $TiCl_4$, CH_4 and H_2 gases as source gases, and their corrosion behaviour was examined in a Br_2–O_2–Ar atmosphere. The following results were obtained.

1. CVD TiC films were obtained in the range between $T_{dep} = 1250$ and 1400 K, and this appropriate T_{dep} range became narrower with increasing $CH_4/TiCl_4$ ratios.

2. The deposition rate increased with increasing T_{dep}, $CH_4/TiCl_4$ ratio and $TiCl_4$ vapour flow rate. The largest deposition rate was $4\,nm\,s^{-1}$ at $T_{dep} = 1273$ K, $CH_4/TiCl_4$ ratio = 17 and $TiCl_4$ vapour flow rate = $4.2 \times 10^{-7}\,m^3\,s^{-1}$.

3. CVD TiC films indicated several kinds of preferred orientation. The dominant orientation changed from (1 1 0) to (1 1 1) with increasing $CH_4/TiCl_4$ ratio, independent of T_{dep} and $TiCl_4$ vapour flow rate.

4. The corrosion of TiC-coated SUS304 in the Br_2–O_2–Ar atmosphere at 973–1173 K was mainly explained by the oxidation of TiC films and that of SUS304 substrates through microcracks in the TiC film.

5. When P_{O_2} was less than 0.1 kPa, weight loss was observed due to the formation of volatile iron and titanium bromides. When P_{O_2} was more than 0.1 kPa, protective oxide scales formed and the weight gain obeyed a parabolic law. This behaviour can be explained by thermodynamic calculations.

6. The corrosion rates (parabolic rate constants, K_p) increased with increasing P_{O_2}, T_{cor} and P_{Br_2}. The apparent activation energy calculated from K_p was 120–160 $kJ\,mol^{-1}$. This value may correspond with the activation energy for diffusion of oxygen in the oxide scales.

Acknowledgement

This research was supported in part by the Grant-in-Aid for Scientific Research on Priority Areas, from the Ministry of Education, Science and Culture, under Contract no. 63 603 505.

References

1. H. KAMEYAMA and K. YOSHIDA, *Jpn. J. Chem. Soc.* (6) (1980) 1060.
2. Y. KONNO, *Bull. Jpn. Inst. Metals* **27** (1988) 110.
3. B. TSUJINO and T. OKI, *J. High Temp. Soc. Jpn* **15** (1989) 227.
4. K. IZUMI, M. MURAKAMI, T. DEGUCHI, A. MORITA, N. TOHGE and T. MINAMI, *J. Mater. Sci.*, in press.
5. C. F. POWELL, J. H. OXLEY and J. M. BLOCHER Jr, "Vapor Deposition" (Wiley, New York, 1966) p. 512.
6. T. HIRAI, K. NIIHARA and S. HAYASHI, *Ceramics* **13** (1978) 861.
7. R. LJUNGQVIST, in "Proceedings of the 3rd International Conference on Chemical Vapor Deposition", edited by F. A. Glaski (Electrochemical Society, Princetown, 1972) p. 383.
8. H. ITOH, M. DONNDA and K. SUGIYAMA, *Kinzoku-Hyoumenn-Gijutsu* **35** (1984) 590.
9. F. K. LOTGERING, *J. Inorg. Nucl. Chem.* **9** (1959) 113.
10. A. DERRE, M. DUCARROIR and F. TEYSSANDIER, in "Proceedings of the 10th International Conference on Chemical Vapor Deposition", edited by G. W. Cullen (Electrochemical Society, Pennington, NJ, 1987) p. 1190.
11. T. TAKAHASHI, K. SUGIYAMA and T. TOMITA, *J. Electrochem. Soc.* **114** (1967) 1230.
12. F. BROSSA, J. BOHDANSKI, J. ROTH and A. P. MARTINELLI, *J. Nucl. Mater.* **93/94** (1980) 474.
13. S. G. YOON, H. G. KIM and J. S. CHUN, *J. Mater. Sci.* **22** (1987) 2629.
14. C-C. JIANG, T. GOTO and T. HIRAI, *ibid.* **25** (1990) 1086.
15. T. HIRAI, T. GOTO and T. KAJI, *Yogyo-Kyokai-Shi* **9** (1983) 502.
16. N. A. PANGAROV, *Electrochem. Acta* **9** (1964) 721.
17. P. J. M. STRATEN, M. M. MICHORIUS and G. VERSPUI, in "Proceedings of the 4th European Conference on Chemical Vapor Deposition", edited by J. Bolem, G. Verspui and L. R. Wolff (Philips Center for Manufacturing Technology, Eindhoven, Netherlands, 1983) p. 553.
18. T. TAKAHASHI, K. SUGIYAMA and K. TOMITA, *Kinnzoku-Hyoumenn-Gijutsu* **18** (1967) 264.
19. S. TSUCHIYA, T. SUZUKI and O. TERADA, *Powders Powder Metall.* **34** (1987) 277.
20. Y. SAITO, H. KIMURA, T. MURAYAMA and T. ATAKE, International Meeting on "Advances in Materials", Vol. 4, edited by K. Nii, Y. Saito and Y. Yoshimura (Materials Research Society, Pittsburg, PA, 1989) p. 395.
21. T. M. BESMANN, Oakridge National Laboratory Technical Report ORNL/TM-5775 (April, 1975).
22. D. R. STULL, H. PROPHET (eds), "JANAF Thermochemical Tables", 2nd Edn, no. NSRDS-NBS-37, US Government Printing Office, Washington, DC, 1971).